J Mater Sci: Mater Med (2013) 24:161–169
DOI 10.1007/s10856-012-4770-8

Surface modification of zirconium by anodisation as material for permanent implants: in vitro and in vivo study

A. Gomez Sanchez · J. Ballarre · J. C. Orellano · G. Duffó · S. Ceré

Received: 2 May 2012 / Accepted: 17 September 2012 / Published online: 29 September 2012

Abstract The potential use of anodised zirconium as permanent implant has been investigated. Zirconium was anodised at constant potential between 3 and 30 V in H_3PO_4. Electrochemical assays were conducted in simulated body fluid solution (SBF) in order to evaluate the effect of the surface oxide on the corrosion resistance in vitro after 30 days of immersion. The rupture potential increases when increasing thickness of the anodic surface film. The increase in the barrier effect when increasing anodising potential is also verified by EIS. Anodisation in H_3PO_4 proved to increase the apatite formation capability of zirconium in a single step. In vivo bone formation was also analysed by implanting the modified materials in Wistar rats. Anodised Zr presents higher corrosion resistance in SBF in all the studied immersion times when compared with non anodised Zr. Additionally, in vivo experiments evidence bone generation and growth in contact with zirconium implants both in the as-received and anodised condition.

A. Gomez Sanchez · J. Ballarre · S. Ceré (✉)
División Corrosión-INTEMA, Universidad Nacional del Mar del Plata-CONICET, Juan B. Justo 4302, B7608FDQ Mar del Plata, Argentina
e-mail: smcere@fi.mdp.edu.ar

J. C. Orellano
Servicio de Ortopedia y Traumatología, Hospital Interzonal General de Agudos Oscar Alende, 7600, Mar del Plata, Argentina

G. Duffó
Departamento de Materiales, Comisión Nacional de Energía Atómica CONICET, Av. Gral. Paz 1499, (1650) San Martín, Buenos Aires, Argentina

G. Duffó
Universidad Nacional de Gral. San Martín, Av. Gral. Paz 1499, (1650) San Martín, Buenos Aires, Argentina

1 Introduction

Valve metals are receiving increasing attention both as alloying components of titanium and as base materials for biomedical applications. Aluminum and vanadium are being substituted by niobium, zirconium and tantalum in biomedical titanium alloys because of their apparent relation with certain severe affections [1, 2]. Some of the alloys being currently studied are Ti–35Nb–7Zr–5Ta, Ti–50Zr %, Ti6Al7Nb and Ti5Al2.5Fe [3–6]. In these alloys, lower metallic ion release than in the Ti–6Al–4V alloy or pure Ti has been found [7, 8].

The promising results of zirconium obtained in some in vitro and in vivo studies have pointed out this metal as a potential material for permanent implants [9–12]. The good performance of zirconium has been mainly attributed to its surface oxide film. The presence on a native ZrO_2 oxide (zirconia) on zirconium surface determines the low corrosion rate of the material, and therefore the low metal ion release to the biological media [13–16]. Moreover, zirconia, as a bulk ceramic material is widely used in dental applications due to its excellent biocompatibility and proven capability to facilitate the osseointegration process [17–21].

Increasing bioactivity while keeping low corrosion is one the main objectives of most of the research being performed on metallic materials for permanent implant applications. It has been extensively proved that the success or failure of the osseointegration process is determined by the surface characteristics in different space length

scales [6, 22–25], and those materials where osseointegration occurs, have a lower implant replacement rate [6].

Surface modification induced by anodisation in the conditions presented in this work corresponds to a surface design criteria based on the modification of chemical and topological features in the nanometric range with the aim of promoting osseointegration of zirconium permanent implants. Since an additional requirement of metal implants is the corrosion resistance in body fluids for long periods, the electrochemical in vitro response of anodised zirconium was systematically studied in order to determine the effect of the surface modification process on the corrosion resistance of this metal. Precipitates on anodised zirconium samples, detected after 30 days of immersion in SBF were characterized by means of Raman spectroscopy. The osseointegration capability was also evaluated, by means of in vivo implantation of anodised zirconium implants in Wistar rats, where histological analysis of bone formation was performed.

2 Experimental

2.1 Material and anodising treatment

In vitro experiments were carried out using commercially pure zirconium sheets (99.5 % Roberto Cordes S.A., Argentina) from which 20 × 15 × 0.127 mm specimens were cut. The electrodes were anodised for 60 min in 1 mol L^{-1} H_3PO_4 at constant potentials between 3 and 30 V. The sample conditioning and oxide growth details were previously reported [26].

Wire (diameter: 1 mm) samples were anodised at 30 V with the same procedure employed on sheets, to be used as permanent implants in the in vivo experiments.

2.2 Simulated body fluid solution (SBF)

Electrochemical and immersion tests were performed in a solution with ion concentration similar to blood plasma, that has been extensively used to evaluate the in vitro behavior of biomaterials [27, 28]. All reagents were provided by Sigma-Aldrich (analytical grade, 85.0 %) and ultrapure water (18.2 MΩ cm, Millipore) was used throughout. The solution was buffered to pH 7.4 with concentrated HCl and tris(hydroxymethyl)aminomethane (tris).

2.3 Electrochemical studies

Zirconium electrodes in the as-received condition and anodised at different potentials were electrochemically studied in SBF using a conventional three electrode cell with a saturated calomel electrode (Radiometer Analytical, France) as reference and a platinum wire as counter electrode. Measurements were performed after 24 h of immersion in SBF. Before each measurement, the potential was left to stabilise for 40 min at open circuit potential (OCP). A Reference 600^{TM} Potentiostat–Galvanostat-ZRA (Gamry Instruments, USA) was used and potentiodynamic polarisation curves were measured from the OCP to 1.5 V or until the current density reached a value of 10^{-2} A cm^{-2}, and backwards at a sweep rate of 0.002 Vs^{-1}.

Electrochemical impedance spectroscopy (EIS) measurements were carried out using a PCI4 750/potentiostat/galvanostat/ZRA^{TM} (Gamry Instruments, USA). The amplitude of the perturbation signal was 10 mV rms and the impedance was measured between 10^{-2} and 10^{6} Hz. The impedance data was fitted to equivalent circuit models with Zplot for Windows software [29].

Anodic polarization and EIS measurements were repeated after 30 days of immersion in SBF for zirconium in the as-received condition and anodised at 30 V.

2.4 Immersion test

Zirconium samples in the as-received condition and anodised at 30 V were maintained in SBF following the recommendations of the ISO 23317:2007(E) standard [30]. The specimens were kept in SBF solution for 30 days at a constant temperature of 37 °C. The sample area (in mm^2) to the solution volume (in ml) ratio was set equal to 10 [31]. After 30 days the surface was assessed by Raman spectroscopy.

2.5 Surface characterization

The crystalline phases corresponding to precipitates on anodised zirconium were determined by Raman spectroscopy using an Invia Reflex confocal Raman microscope (Renishaw, UK). The Raman spectra were obtained using a 514 nm argon laser with a 50× objective lens. No thermal effects were observed for the samples during these measurements.

2.6 In vivo experiments

In vivo experiments were conducted on 4 Wistar adult rats (weighted 350 ± 50 g), according to the codes and rules of the Interdisciplinary Bio-Ethics Program University of Mar del Plata (April 2005). The surgical and preparation samples procedure was described before [32, 33]. Briefly, the as-received and anodised Zr implants wires of 1.5 cm length were sterilized in an autoclave for 20 min at 121 °C, rats were anaesthetized with fentanyl citrate and droperidol according to their weight. Zirconium wires corresponding

to the as-received condition and anodised at 30 V were placed by press fit into the tibia, extending them into the medullar canal. Both conditions were implanted on each animal, for the sake of comparison. The animals were sacrificed with an overdose of intraperitoneal fentanyl citrate and droperidol after 60 days. Conventional X-ray radiographs were taken before retrieving the samples for control purposes. The bones with implants were ablated, cleaned from surrounding soft tissues and fixed in neutral 10 wt % formaldehyde for 24 h. Then they were dehydrated in a series of ethanol–water mixture and finally embedded in methyl methacrylate (PMMA) solution and polymerized. The PMMA embedded blocks were cut with a low speed diamond blade saw (Buehler GmbH), to obtain 100–150 μ thickness sections.

Histological sections were stained with toluidine blue stain solution in order to analyse the soft tissue and the bone lining cells [34]. The stained sample sections were observed using optical light microscopy (Olympus, BH2, Japan).

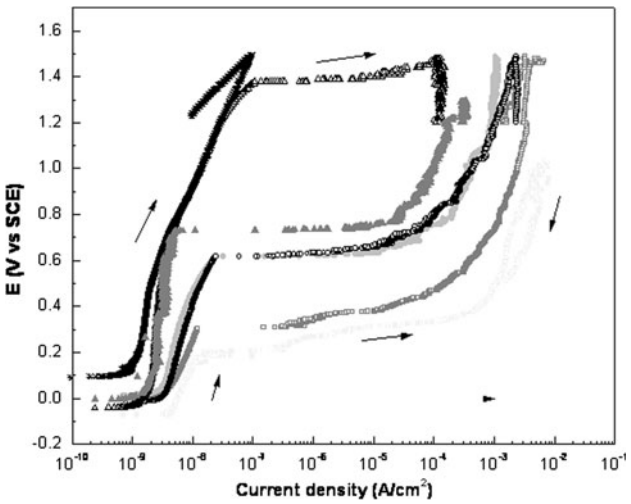

Fig. 1 Anodic polarization curves after 24 h of immersion in SBF solution of (*filled square*) Zr as-received, and anodised at: (*open square*) 3 V, (*filled circle*) 6 V, (*open circle*) 9 V, (*filled triangle*) 18 V, (*open triangle*) 24 V, (*Asterisk*) 30 V

3 Results and discussion

A complete surface and electrochemical characterisation of zirconium before and after anodisation in phosphoric acid was previously presented [26, 35]. It was demonstrated that anodic oxides forms isolated irregular structures on the surface, increasing size and coverage when increasing the anodisation voltage. Monoclinic ZrO_2 was the only crystallographic phase detected in anodised zirconium, with the incorporation of phosphates from the anodising electrolyte, meanwhile tetragonal ZrO_2 was the main feature detected for the as-received condition. It was also determined a characteristic colour for each anodising potential and it was verified by EIS the thickness increase of the anodic films when rising anodic voltage [26, 35]. Therefore, it was proven that anodisation induces both chemical and topological changes on zirconium.

3.1 Electrochemical tests

3.1.1 Anodic polarization

Anodic polarization curves after 24 h immersion in SBF solution of zirconium as-received and anodised at different potentials are shown in Fig. 1.

The corrosion potential (E_{corr}) moves in the positive direction when increasing the anodising potential, evidencing a nobler surface of the anodic films when increasing its thickness [36, 37]. The same tendency is observed when analyzing the rupture potential. The rupture of the passive film during anodic polarization was observed in all the studied conditions but the anodised at 30 V, where the material remains in the passive state during the anodic polarization test in the domain of the assayed potentials in this study. This behavior can be attributed to an increase in the anodic oxide coverage and thickness of the film obtained at this potential.

An increase in the rupture potential, together with decreasing passive current density of one order of magnitude between as-received zirconium and zirconium anodised at 30 V is observed. The localized rupture of the surface protective film and further anodic dissolution of zirconium metal forming pits mainly on the edges of the samples evidences the aggressiveness of this simulated biological media. The susceptibility of zirconium to localized corrosion during anodic polarization was previously reported in other simulated biological media, including Hank's solution, phosphate buffer solution and Ringer solution [38, 39]. In those works, alloying elements seem to increase the corrosion resistance of zirconium.

The aggressive effect of chloride ions on zirconium alloys was studied by El-Mahdy et al. [40]. They determined that chloride ion induces localized corrosion during anodic polarization. Hiromoto et al. determined that Zr65Al7.5-Ni10Cu17.5 zirconium alloy is susceptible to both localized and general corrosion in chloride containing media, and stated that the effect is independent of the pH [41].

3.1.2 EIS

Figure 2 shows Bode plots of zirconium as-received and anodised at different potentials, after 24 h of immersion in SBF. An increase of total the impedance of the system

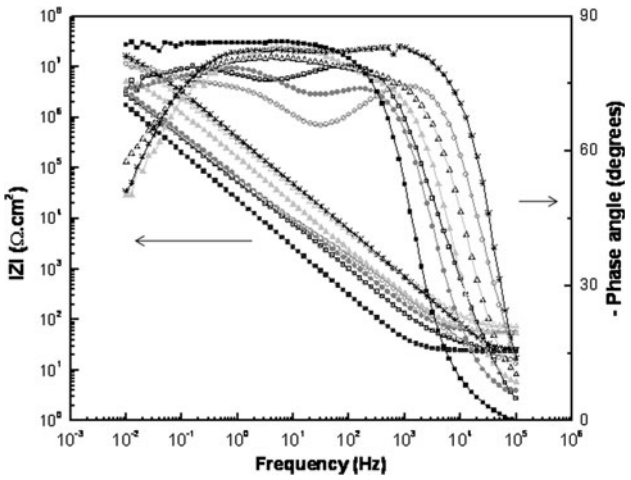

Fig. 2 Bode plots after 24 h in SBF solution of (*filled square*) Zr as-received, and anodised at: (*open square*) 3 V, (*filled circle*) 6 V, (*open circle*) 9 V, (*filled triangle*) 18 V, (*open triangle*) 24 V, (*Asterisk*) 30 V. *Solid line* shows the equivalent circuit fitting

when increasing the anodising potential is observed, together with a shift to higher frequencies in the high frequency domain of the phase angle versus frequency plot, raising the angle close to 90°. Both characteristics of the EIS response can be related to an increase of the barrier effect of the anodic films obtained at higher anodising potentials, which is in agreement with the decrease in current density observed by anodic polarization curves.

EIS results of zirconium as-received can be accurately reproduced with the equivalent circuit presented in Fig. 3a. This circuit represents the response of a protective dense layer on the metal surface that acts as a barrier between the metal and the solution [42–44]. In the circuit, Re represents the solution resistance, whereas Q and R represent the pseudocapacitance and the resistance associated to the native oxide respectively.

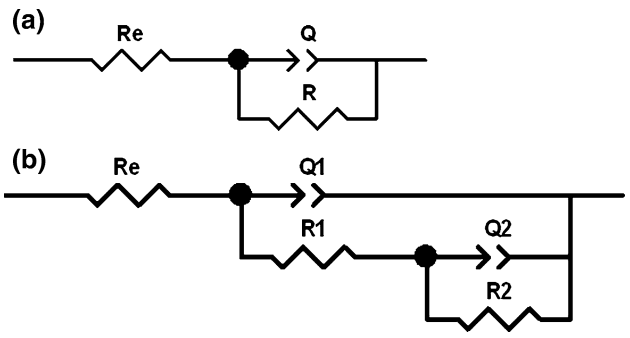

Fig. 3 **a** Equivalent circuit used to fit the experimental results of as-received zirconium. **b** Equivalent circuit used to fit the experimental results of anodised zirconium

All anodised samples could be fitted using the equivalent circuit shown in Fig. 3b, where the sub-indices 1 and 2 in the circuit components correspond to the outer and inner oxides respectively. In this representation, the inner layer, in contact with the metal substrate acts as a dense structure while the outer is a more porous layer in contact with the electrolyte. This circuit has been used to describe a double layer structure of surface films in different systems, including titanium surface oxides in contact with SBF solutions [45–48].

For the simulation of impedance plots, a constant phase element impedance contribution (Z_{CPE}) was used instead of an ideal capacitor to explain the deviations from a slope of -1 in the modulus Bode plot. The impedance of a constant phase element (Z_{CPE}) is given by [49]:

$$Z_{CPE} = 1/Q(j\omega)^{\alpha} \quad (1)$$

where Q is a parameter independent of frequency. When $\alpha = 1$, Q has units of capacitance (F cm^{-2}) and represents the capacitance of the interface. When $\alpha < 1$ the system shows a behaviour that can be attributed to surface heterogeneity or to a distribution of time constants and Q have the units $s^{\alpha}\Omega^{-1}$ cm^{-2}. α is a coefficient associated with system homogeneity [49–53].

Taking into account the morphology of the oxide films grown on zirconium observed by SEM and considering the surface film as a blocking electrode [53] the model developed by Brug et al. [51] was used to determine the effective capacitance of zirconium when immersed in SBF solution. C_{eff} values where therefore determined by:

$$C_{eff} = Q^{1/\alpha} R_e^{(1-\alpha)/\alpha} \quad (2)$$

where R_e is the electrolyte resistance and all the other parameters have the same meaning as in Eq. (1) [53].

The decrease of the effective capacitance when increasing anodising potential is evidenced in Table 1 and Fig. 6, and can be related to the increase of the surface oxide film thickness. However, since the effective capacitance values are minor than those reported for the anodic oxides in contact with the anodising solution [35], the values obtained in SBF may also include the effect of interactions between the surface films and the solution, as adsorbed species from the electrolyte incorporated to the surface.

3.1.3 Electrochemical behavior after 30 days of immersion in SBF solution

3.1.3.1 Anodic polarization Anodic polarization curves of zirconium both in the as-received condition and anodised at 30 V, after 30 days of immersion in SBF are shown in Fig. 4a, b. In both conditions an increase in current density in the passive range is observed after the

Table 1 Effective capacitance of zirconium surface film anodised at different potentials after 24 h immersion in SBF solution

Anodising potential (v)	0	3	6	9	12	18	24	30
C_{eff} (F cm^2)	$4.2\ 10^{-8} \pm 0.2\ 10^{-8}$	$1.1\ 10^{-8} \pm 0.3\ 10^{-8}$	$6.8\ 10^{-7} \pm 0.2\ 10^{-7}$	$4.0\ 10^{-7} \pm 0.2\ 10^{-7}$	$3.8\ 10^{-7} \pm 0.2\ 10^{-7}$	$3.5\ 10^{-7} \pm 0.5\ 10^{-7}$	$1.7\ 10^{-7} \pm 0.2\ 10^{-7}$	$3.3\ 10^{-7} \pm 0.6\ 10^{-7}$

immersion period. This is indicative of certain degree of deterioration of the passive film during immersion. However, after 30 days, the passive current density remains in low values. Moreover, anodised zirconium presents after 30 days of immersion in SBF solution similar passive current density compared to untreated metal, but lower current density in the surrounding of the corrosion potential besides, anodized Zr shows a higher rupture potential indicating a broad range of stability of this material.

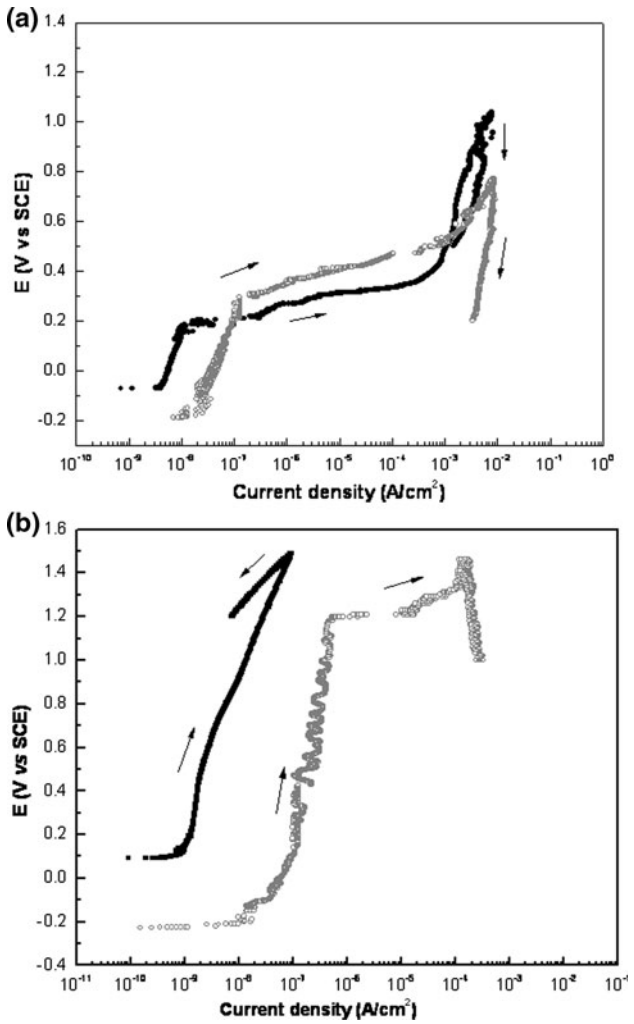

Fig. 4 Anodic polarization curves of (a) As-received zirconium after (*filled circle*) 24 h and (*open circle*) 30 days of immersion in SBF solution. (b) Zirconium anodised at 30 V after (*filled circle*) 24 h and (*open circle*) 30 days of immersion in SBF solution

3.1.4 EIS

Figure 5 shows Bode plots comparing EIS results of zirconium as-received and anodised at 30 V after 24 h and 30 days of immersion in SBF. A decrease in the total impedance when increasing immersion time is observed in both surface conditions, that evidences a deterioration of the barrier effect of both surfaces with immersion in SBF solution. However, after the prolonged immersion time, anodised samples evidence higher impedance values than

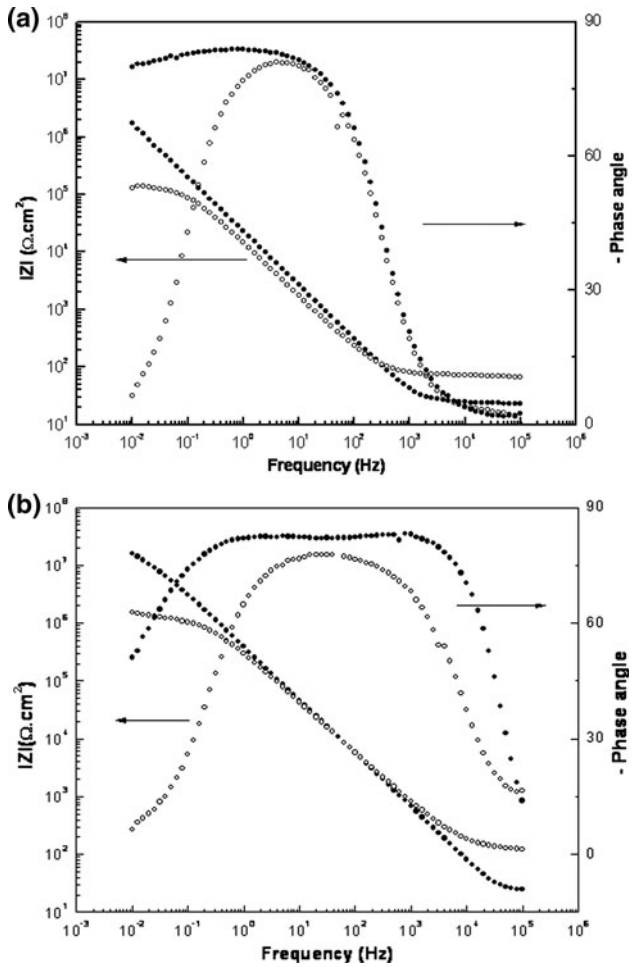

Fig. 5 EIS results of (a) As-received zirconium after (*filled circle*) 24 h and (*open circle*) 30 days of immersion in SBF. (b) Zirconium anodised at 30 V after (*filled circle*) 24 h and (*open circle*) 30 days of immersion in SBF

the as-received condition. Zirconium anodised at 30 V presents a shift in the phase angle versus frequency plot to the higher frequencies region together with a decrease in phase angle at low frequencies. These two characteristics can be related to the blocking of surface defects with porous deposits (which lead to the decrease in the total impedance) that conducts to an increase of the thickness of the deposits (in accordance with the phase angle shift) [54]. These results are in good agreement with the deposits of Ca–P rich compounds determined with SEM [26].

Effective capacitance of surface films after 30 days of immersion present differences from those obtained after 24 h of immersion (Fig. 6). In the as-received material, the electrolyte-film-metal interaction is represented by an increase in capacitance, related to the deterioration process occurring on the native oxide film that probably includes the filling of the oxide pores with the electrolyte. On the contrary, in anodised zirconium, the capacitance decreases. The later can be associated to an increase in the surface layer thickness, and to permittivity changes that can be related to the presence of Ca–P rich precipitates covering the oxide surface film, as was observed by SEM and further corroborated by Raman (see Sect. 3.2) [26].

3.2 Surface modifications after immersion in SBF

In a previous work, precipitates of acicular crystals on zirconium anodised at 30 V after 30 days of immersion in SBF were observed by SEM and the presence of Ca, Na, K and Mg was detected with EDS [26]. On the contrary, on as-received zirconium neither morphology changes nor Ca compounds were detected on the surface after immersion [26].

Figure 7 shows the Raman spectra corresponding to the precipitates formed on zirconium anodised at 30 V and the comparison with the spectrum of the same material without immersion in SBF. Besides the peaks corresponding to the zirconium oxide, three new bands appear, at 430–438, 551–557 and 986–1014 cm^{-1}, and a shoulder at 1,043 cm^{-1}. These bands can be attributed, to vibrational modes of phosphates in apatites [55–57]. In accordance with EDS and SEM results [26], no peaks assignable to Ca–P compounds were detected on untreated zirconium after 30 days of immersion in SBF solution.

Electrochemical surface modification processes to promote Ca–P rich compounds precipitation during immersion in simulated body solutions are being recently explored. Uchida et al. first determined this kind of precipitates on zirconium treated in alkaline media [58]. The alkaline treatment was also applied to titanium alloys containing zirconium [59], whereas Tsutsumi et al. performed cathodic polarization treatments in Hanks solution to obtain Ca–P compounds on the metal surface [60, 61]. Recently, Ha et al. have studied the increase in biocompatibility of zirconium by means of micro arc oxidation treatments followed by alkaline treatment [62]. All the above named treatments were able to induce Ca–P rich compounds on the metal surface. However, the corrosion stability of these thick and porous films has not been reported. Compared to those surface modification processes, anodisation in H_3PO_4 showed in this work proved to increase the apatite formation capability of zirconium in a single step, without any further chemical treatment or cathodic polarization required to induce the precipitation of Ca–P compounds.

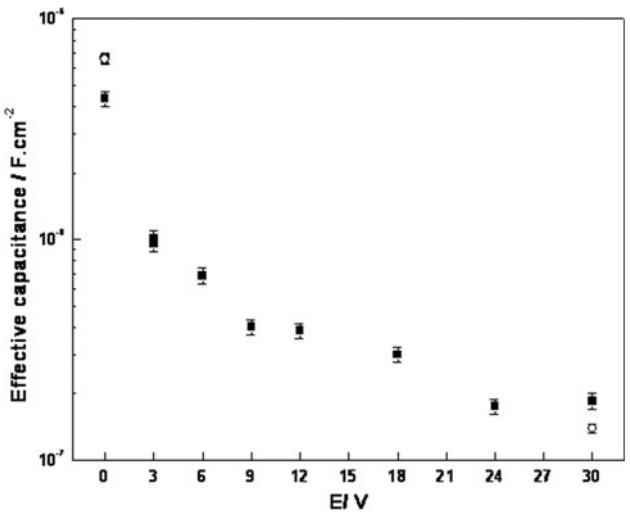

Fig. 6 Effective capacitance of surface films on zirconium anodized at different potentials after immersion in SBF during (*filled square*) 24 h and after (*open circle*) 30 days of immersion

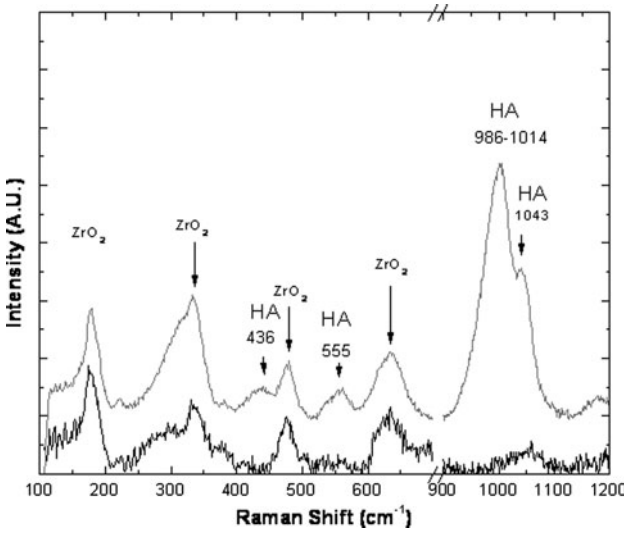

Fig. 7 Raman spectra of Zr anodised at 30 V: *thick line* prior to immersion in SBF solution, *shaded line* after 30 days of immersion in SBF solution

3.3 In vivo test

Figure 8a–c show the optical microscopic images of Giemsa stained sections of the as-received and anodised zirconium samples after 60 days of implantation in rat tibia.

In both conditions a newly formed tissue can be seen at the periphery of the implants, showing a bioactive and behaviour, similar to the results obtained by other authors when comparing the bone formation around zirconium metal without any further treatment and zirconium with a ZrO_2 coating by sol gel [63]. After 60 days of implantation, the newly-formed tissue around the implant is continuous, presenting osteocytic lacunae, as it is showed with an arrow in Fig. 8c, also it can be observed an osteoblast-rich surface at both sides of the newly-growth tissue, which shows a continuous bone growth.

Further work is being developed in order to characterize the quality and degree of mineralization of the bone formed with both surface treatments.

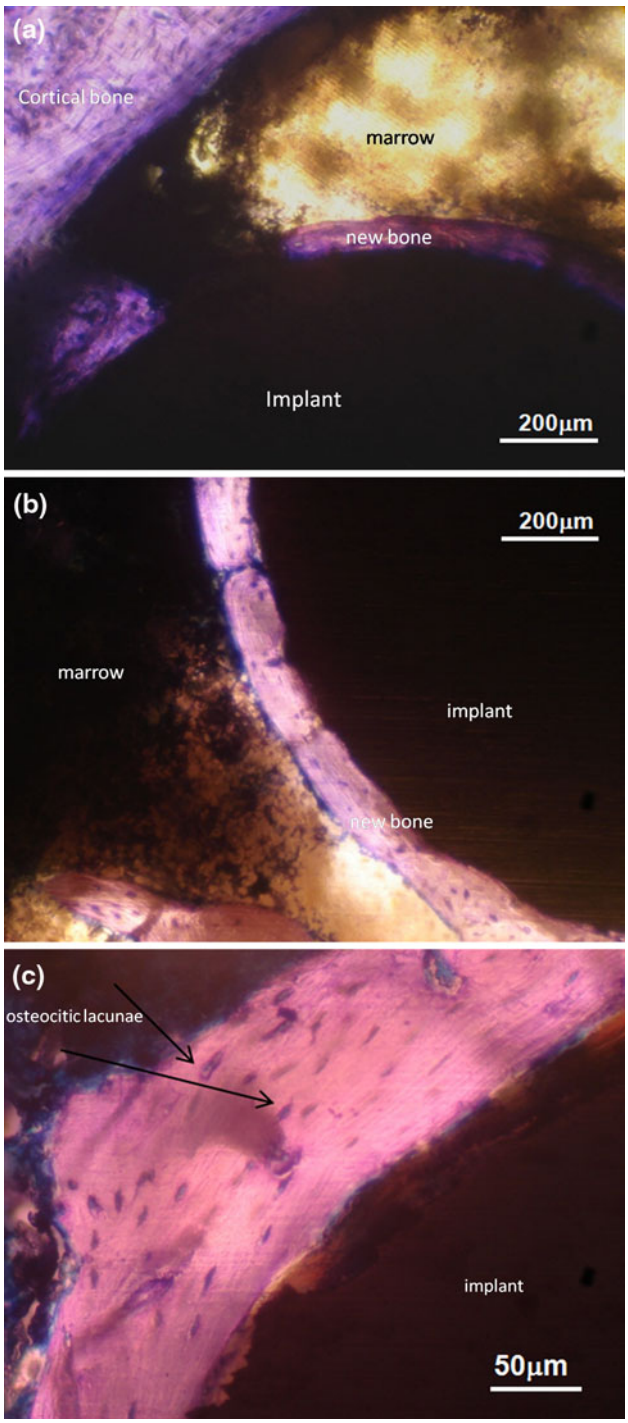

Fig. 8 Optical microscopic image of Giemsa stained histology section showing the implant and the newly formed bone around **a** as-received and **b** the anodised Zr samples after 60 days (10×). **c** Detailed optical microscopic image of Giemsa stained histology section of the anodised zirconium showing the bone growth around the implant (20×). The *arrows* indicates the presence of osteocitic lacunae

4 Conclusions

Zr presents a low passive current density for all the anodising conditions studied after 24 h of immersion in SBF, although shows susceptibility to localized corrosion during anodic polarization for all conditions but 30 V. The rupture potential increases when increasing thickness of the anodic surface film. The increase in the barrier effect when increasing anodising potential is also verified by EIS.

After 30 days of immersion in SBF solution, the electrochemical tests demonstrated certain degree of deterioration of the surface protective film on zirconium, in both the as-received and the anodised at 30 V samples. Although, the impedance modulus remain showing a higher corrosion resistance for the anodised condition with respect to the as-received zirconium.

Immersion tests demonstrated the presence of apatite on the surface of anodised zirconium after 30 days in SBF. Anodisation in H_3PO_4 showed to increase the apatite formation ability of zirconium in a single step, without any further treatment in order to induce the precipitation of Ca–P compounds.

Surface modification of zirconium by anodisation has proved to be a treatment that can keep corrosion parameters in low values while is able to promote Ca–P compounds precipitation on the surface endorsing the bioactivity of the material and promoting bone regeneration. In vivo experiments evidence bone generation and growth in contact with zirconium implants both in the as-received and anodised conditions. Although osseointegration is observed in anodised and as-received materials, the bone quality of the generated bone has to be analyzed in terms of bone maturity and cell proliferation.

It is worth noting that in vitro tests regarding the apatite formation ability is not in agreement with the in vivo results presented, since according to the former, as-received Zr does not show "signs of being an apatite forming surface" in vitro, while the bone formation around the implants is clearly verified. This discrepancy reinforces the importance of the animal model studies related to bone formation surfaces.

Acknowledgments The support from Consejo Nacional de Investigaciones Científicas y Técnicas, Agencia Nacional de Promoción Científica y Tecnológica (PICT 0550/07) and Universidad Nacional de Mar del Plata (15G/270), Argentina, is gratefully acknowledged. The authors also acknowledge Drs. Valcarce and Valdes for the Raman measurements.

References

1. Nag S, Banerjee R, Fraser HL. Microstructural evolution and strengthening mechanisms in Ti–Nb–Zr–Ta, Ti–Mo–Zr–Fe and Ti–15Mo biocompatible alloys. Mater Sci Eng C. 2005;25:357–62.
2. Lopez MF, Gutierrez A, Jimenez JA. Surface characterization of new non-toxic titanium alloys for biomedical characterization. Surf Sci. 2001;482–485:300–5.
3. Taddei EB, Henriques VAR, Silva CRM, Cairo CAA. Production of new titanium alloy for orthopedic implants. Mater Sci Eng C. 2004;24:683–7.
4. Li SJ, Yang R, Niinomi M, Hao YL, Cui YY. Formation and growth of calcium phosphate on the surface of oxidized Ti–29Nb–13Ta–4.6Zr alloy. Biomaterials. 2004;25:2525–32.
5. Li SJ, Yang R, Li S, Hao YL, Cui YY, Niinomi M, Guo ZX. Wear characteristics of Ti–Nb–Ta–Zr and Ti–6Al–4V alloys for biomedical applications. Wear. 2004;257:869–76.
6. Navarro M, Michiardi A, Castaño O, Planell JA. Biomaterials in orthopaedics—review. J R Soc Int. 2008;5:1137–58.
7. Okazaki Y, Gotoh E. Comparison of metal release from various metallic biomaterials in vitro. Biomaterials. 2005;26:11–21.
8. Lopez MF, Gutierrez A, Jimenez JA. In vitro corrosion behavior of titanium alloys without vanadium. Electrochim Acta. 2002;47:1359–64.
9. Saldaña L, Méndez-Vilas A, Jiang L, Multigner M, González-Carrasco JL, Pérez-Prado MT, González-Martín ML, Munuera L, Vilaboa N. In vitro biocompatibility of an ultrafined grained zirconium. Biomaterials. 2007;28:4343–54.
10. Cabrini R, Guglielmotti MB, Almagro JC. Histomorphometry of initial bone healing around zirconium implants in rats. Implant Dent. 1993;2:264–7.
11. Costa OR, Guglielmotti MB, Rimoli E, Cabrini RL. Use of zircalloy to induce bone regeneration. A 2-year follow-up study. Acta Odont Latinoam. 1994;8:17–26.
12. Guglielmotti MB, Guerrero C, Cabrini RL. Chronodynamic evaluation of the stages of osseointegration in zirconium laminar implants. Acta Odont Latinoam. 1997;10:11–23.
13. Hiromoto S, Hanawa T. Re-passivation current of amorphous Zr65Al7.5Ni10Cu17.5 alloy in a Hanks' balanced solution. Electrochemica Acta. 2002;47:1343–9.
14. Hanawa T. In vivo metallic biomaterials and surface modification. Mater Sci Eng A. 1999;267:260–6.
15. Kohn DH. Metals in medical applications. Curr Opin Solid State Mater Sci. 1998;3:309–16.
16. Patel AM, Spector M. Tribological evaluation of oxidized zirconium using an articular cartilage counterface: a novel material for potential use in hemiarthroplasty. Biomaterials. 1997;18:441–7.
17. Piconi C, Maccauro G. Zirconia as a ceramic biomaterial—review. Biomaterials. 1999;20:1–25.
18. Carinci F, Pezzetti F, Volinia S, Francioso F, Arcelli D, Farina E, Piattelli A. Zirconium oxide: analysis of MG63 osteoblast-like cell response by means of a microarray technology. Biomaterials. 2004;25:215–28.
19. Deville S, Chevalier J, Fantozzi G, Bartolomé JF, Requena J, Moya JS, Torrecillas R, Díaz LA. Low-temperature ageing of zirconia-toughened alumina ceramics and its implication in biomedical implants. J Eur Ceram Soc. 2003;23:2975–82.
20. Chevalier J, Gremillard L. Ceramics for medical applications: a picture for the next 20 years. J Eur Ceram Soc. 2008;29:1245–55.
21. Adolfsson E, Hermansson L. Zirconia fluorapatite materials produced by HIP. Biomaterials. 1999;20:1263–7.
22. Mendonça G, Mendonça DBS, Aragão FJL, Cooper LF. Advancing dental implant surface technology—from micron to nanotopography. Biomaterials. 2008;29:3822–35.
23. Davies JE. Bone bonding at natural and biomaterials surfaces. Biomaterials. 2007;28:5058–67.
24. Oliveira AL, Mano JF, Reis RL. Nature-inspired calcium phosphate coatings: present status and novel advances in the science of mimicry. Curr Opin Solid State Mater Sci. 2003;7:309–18.
25. Barrere F, Snel MME, van Blitterswijk CA, de Groot K, Layrolle P. Nano-scale study of the nucleation and growth of calcium phosphate coating on titanium implants. Biomaterials. 2004;25:2901–10.
26. Gomez Sanchez A, Schreiner W, Duffó G, Ceré S. Surface characterization of anodized zirconium for biomedical applications. Appl Surf Sci. 2011;257:6397–405.
27. Kokubo T, Ito S, Huang ZT, Hayashi T, Sakka S, Kitsugi T, Yamamuro T. Ca, P-rich layer formed on high-strength bioactive glass–ceramic A-W. J Biomed Mater Res. 1990;24:331–43.
28. Kokubo T, Kushitani H, Sakka S. Solutions able to reproduce in vivo surface-structure changes in bioactive glass–ceramic A-W3. J Biomed Mater Res. 1990;24:721–34.
29. Zplot for Windows. Electrochemistry, impedance software operating manual, Part 1. Southern Pines, NC: Scribner Ass. Inc.;1998.
30. International Standard ISO 23317:2007(E), Implants for surgery—in vitro evaluation for apatite-forming ability of implant materials, Switzerland; 2007.
31. Kokubo T, Takadama H. How useful is SBF in predicting in vivo bone bioactivity? Biomaterials. 2006;27:2907–15.
32. Ballarre J, Manjubala I, Schreiner WH, Orellano JC, Fratzl P, Ceré S. Improving the osteointegration and bone-implant interface by incorporation of bioactive particles in sol–gel coatings of stainless steel implants. Acta Biomater. 2010;6:1601–9.
33. Ballarre J, Seltzer R, Mendoza E, Orellano JC, Mai YW, García C, Ceré SM. Morphologic and nanomechanical characterization of bone tissue growth around bioactive sol–gel coatings containing wollastonite particles applied on stainless steel implants. Mater Sci Eng C. 2011;31:545–52.
34. Bradbeer JN, Riminucci M, Bianco P. Giemsa as a fluorescent stain for mineralized bone. J Histochem Cytochem. 1994;42:677–80.
35. Gomez Sanchez A. In vitro and in vivo evaluation of the feasibility of the use of zirconium as a permanent osseointegrable implant material. PhD thesis, Universidad Nacional de General San Martín, Argentina; 2011.
36. Alves VA, Reis RQ, Santos ICB, Souza DG, Gonçalves TF, Pereira-da-Silva MS. In situ impedance spectroscopy study of the electrochemical corrosion of Ti and Ti–6Al–4V in simulated body fluid at 25°C and 37°C. Corros Sci. 2009;51:2473–82.
37. Karthega M, Raman V, Rajendran N. Influence of the potential on the electrochemical behavior of β titanium alloys in Hank's solution. Acta Biomater. 2007;3:1019–23.

38. Branzoi IV, Iordoc M, Codescu M. Electrochemical studies on the stability and corrosion resistance of new zirconium-based alloys for biomedical applications. Surf Interface Anal. 2008;40:167–73.
39. Oliveira NTC, Biaggio SR, Rocha-Filho RC, Bocchi N. Electrochemical studies on zirconium and its alloys Ti–50Zr at.% and Zr–2.5Nb wt% in simulated physiological media. J Biomed Mater Res. 2005;74A:397–407.
40. El-Mahdy GA, Mahmoud SS, EI-Dahan HA. Effect of halide ions on the formation and dissolution behaviour of zirconium oxide. Thin Solid Films. 1996;286:289–94.
41. Hiromoto S, Tsai AP, Sumita M, Hanawa T. Effect of pH on the polarization behavior of Zr65Al7.5Ni10Cu17.5 amorphous alloy in a phosphate-buffered solution. Corros Sci. 2000;42:2193–200.
42. Bardwell JA, McKubre MCH. AC impedance spectroscopy of the anodic film on zirconium in neutral solution. Electrochim Acta. 1991;36:647–53.
43. Patrito EM, Macagno VA. Influence of the forming electrolyte on the electrical properties of anodic zirconium oxide films. Part II. AC impedance investigation. J Electroanal Chem. 1994;375:203–11.
44. Pauporté T, Finne J. Impedance spectroscopy study of anodic growth of thick zirconium oxide films in H_2SO_4, Na_2SO_4 and NaOH solutions. J Appl Electrochem. 2006;36:33–41.
45. Aziz-Kerrzo M, Conroy KG, Fenelon AM, Farell ST, Breslin CB. Electrochemical studies on the stability and corrosion resistance of titanium-based implant materials. Biomaterials. 2001;22:1531–9.
46. Pan J, Thierry D, Leygraf C. Electrochemical impedance spectroscopy study of the passive oxide film on titanium for implant application. Electrochim Acta. 1996;41:1143–53.
47. Ibris N, Mirza Rosca JC. EIS study of Ti and its alloys in biological media. J Electroanal Chem. 2002;526:53–62.
48. de Assis SL, Wolynec S, Costa I. Corrosion characterization of titanium alloys by electrochemical techniques. Electrochim Acta. 2006;51:1815–9.
49. Jorcin JB, Orazem ME, Pébère NP, Tribollet B. CPE analysis by local electrochemical impedance spectroscopy. Electrochim Acta. 2006;51:1473–9.
50. Orazem M, Tribollet B. Electrochemical impedance spectroscopy, the electrochemical society. New York: Wiley; 2008.
51. Brug GJ, Van Den Eeden ALG, Sluyters-Rehbach M, Sluyters JH. The analysis of electrode impedances complicated by the presence of a constant phase element. J Electroanal Chem. 1984;176:275–95.
52. Hsu CH, Mansfeld F. Concerning the conversion of the constant phase element parameter yo into a capacitance. Corrosion. 2001;57:747–8.
53. Hirschorn B, Orazem M, Tribollet B, Vivier V, Frateur I, Musiani M. Determination of effective capacitance and film thickness from constant-phase-element parameters. Electrochim Acta. 2010;55:6218–27.
54. Metikos-Hukovic M, Tkalcec E, Kwokal A, Piljac J. An in vitro study of Ti and Ti-alloys coated with sol–gel derived hydroxiapatite coatings. Surf Coat Technol. 2003;265:40–50.
55. Antonakos A, Liarokapis E, Leventouri T. Micro-Raman and FTIR studies of syntetic and natural apatites. Biomaterials. 2007;28:3043–54.
56. Silva CC, Rocha HHB, Freire FNA, Santos MRP, Saboia kDa, Goes JC, Sombra ASB. Hydroxyapatite screen-printed thick films: optical and electrical properties. Mater Chem Phys. 2005;92:260–8.
57. Müller L, Müller FA. Preparation of SBF with different HCO_3-content and its influence on the composition of biomimetic apatites. Acta Biomater. 2006;2:181–9.
58. Uchida M, Kim HM, Miyaji F, Kokubo T, Nakamura T. Apatite formation on zirconium metal treated with aqueous NaOH. Biomaterials. 2002;23:313–7.
59. Müller FA, Bottino MC, Müller L, Henriques VAR, Lohbauer U, Bressiani AEA, Bressiani JC. In vitro apatite formation on chemically treated (P/M) Ti–13Nb–13Zr. Dent Mater. 2008;24:50–6.
60. Tsutsumi Y, Nishimura D, Doi H, Nomura N, Hanawa T. Cathodic alkaline treatment of zirconium to give the ability to form calcium phosphate. Acta Biomater. 2010;6:4161–6.
61. Tsutsumi Y, Nishimura D, Doi H, Nomura N, Hanawa T. Difference in surface reactions between titanium and zirconium in Hanks' solution to elucidate mechanism of calcium phosphate formation on titanium using XPS and cathodic polarization. Mater Sci Eng C. 2009;29:1702–8.
62. Ha JY, Tsutsumi Y, Doi H, Nomura N, Kim KH, Hanawa T. Enhancement of calcium phosphate formation on zirconium by micro-arc oxidation and chemical treatments. Surf Coat Technol. 2011;205:4948–55.
63. Sollazzo V, Pezzetti F, Scarano A, Piattelli A, Bignozzi CA, Massari L, Brunelli G, Carinci F. Zirconium oxide coating improves implant osseointegration in vivo. Dent Mater. 2008;24:357–61.